Penetration depth limits of *in vivo* confocal reflectance imaging

Colin L. Smithpeter, Andrew K. Dunn, A. J. Welch, and Rebecca Richards-Kortum

We present experiments to predict the maximum penetration depth at which typical biological structures in amelanotic tissue can be detected with confocal microscopy. The detected signal is examined as the signal source strength (index of refraction mismatch), the source depth, and the medium scattering coefficient are varied. The detected background produced by scattering outside the focal volume is examined as the medium scattering coefficient, the depth in the medium, the dimensionless pinhole radius, v_p, and the shape of the scattering phase function are varied. When the system approaches ideal confocal performance ($v_p \simeq 3$), the penetration depth is limited by the signal-to-noise ratio to approximately 3–4 optical depths (OD's) for a 0.05 index mismatch. As v_p increases to 8, the penetration depth is limited by the signal-to-background ratio and is dependent on the scattering coefficient. At $\mu_s = 100$ cm^{-1} ($l_s = 100$ μm) and an index mismatch of 0.05, the maximum penetration depth is approximately 2 OD. © 1998 Optical Society of America

OCIS codes: 110.0110, 120.5700, 290.0290.

1. Introduction

Recently, images of tissues with cellular resolution have been obtained with *in vivo* confocal reflectance microscopy.[1–3] This technique may provide an important new diagnostic method to assess tissue and cellular morphology *in situ*. The confocal system limits the spatial origin of detected photons to near the focal region of the objective lens. In highly scattering media, such as tissue, the ability to image relies on the ability of the confocal system to reject photons that are multiply scattered outside the focal region. For determining the efficacy of confocal imaging for noninvasive diagnosis, it is critical to predict the maximum thickness of highly scattering tissue through which biological signals can be detected before the signal falls below the background level generated by scattering outside the focal volume or the noise floor.

The issue of penetration depth has been addressed previously.[4–6] Izatt *et al.*[4] used single backscatter theory to estimate that penetration depth was limited by the signal-to-background (S/B) ratio to 5 to 8 optical depths (OD's) (OD = $\mu_t *$ depth), depending on the numerical aperture (NA) of the objective. In the near IR portion of the spectrum, the scattering coefficient, μ_s, is much larger than the absorption coefficient, μ_a, and the definition of OD simplifies to $\mu_s *$ depth. Schmitt *et al.*[5] showed that as the OD increases, multiple scattering becomes more important and degrades the ability of a confocal microscope to reject out of focus light beyond that predicted by single-scattering theory. Schmitt *et al.*[5] found experimentally that a highly reflective object could only be detected to a depth of 3–4 OD's, and was limited by the loss of image contrast due to poor rejection of background scattered light. However, as Kempe *et al.*[6] notes, these experiments were performed with a confocal system with a relatively large (8 to 17) normalized pinhole radius, v_p. In optical units, v_p is given by $\pi d_p \mathrm{NA}/\lambda$, where d_p is the diameter of the pinhole, NA is the numerical aperture of the lens to the pinhole, and λ is the illumination wavelength. Using a v_p of 1.3, Kempe *et al.*[6] imaged a highly reflective grating through 6 OD's of scattering and found the penetration depth was limited by the signal-to-noise (S/N) ratio, rather than the S/B ratio.

In the studies described above,[5,6] the signal source provided much stronger reflections than expected from biological tissue. Our previous study[7] with Monte Carlo simulations has shown that index mismatches, rather than changes in bulk scattering or absorption, produce the greatest contrast in confocal images. Typical index mismatches found between cellular components in unpigmented (amelanotic) tis-

The authors are with Biomedical Engineering, University of Texas-Austin, Austin, Texas 78712.

Received 11 August 1997; revised manuscript received 16 January 1998.

0003-6935/98/132749-06$15.00/0

© 1998 Optical Society of America

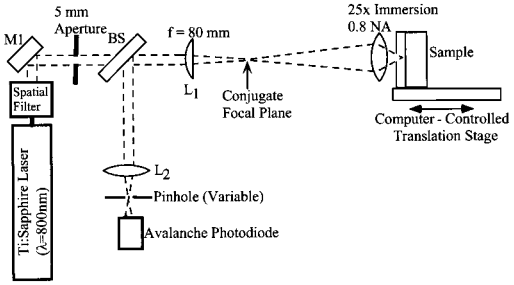

Fig. 1. Experimental setup used to measure the confocal reflected light from tissue phantoms as a function of focal depth within the sample.

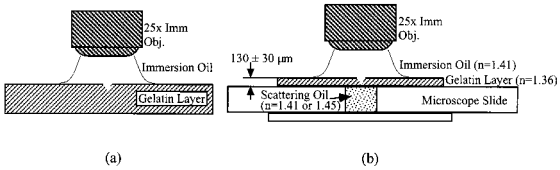

Fig. 2. Tissue phantoms used to measure (a) the background from a uniform scattering layer of gelatin and (b) the signal and the background from uniform layers of gelatin (n = 1.36) and immersion oil (n = 1.41 and 1.45) with equivalent scattering coefficients.

sues are approximately 0.05 and would produce ~3–4 orders of magnitude less signal than a perfect reflector. Even in pigmented tissues where melanin (n = 1.7) provides a strong index mismatch and source of contrast,[3] the expected signal strength is 2 orders of magnitude less than that provided by a perfect reflector. For a 0.05 index of refraction mismatch, our simulations estimated that penetration depth was limited to 2 to 3 OD's by poor rejection of background scattered light. However, this estimate was for a confocal system with a ν_p of 13. As Kempe *et al.*[6] have shown, decreasing ν_p reduces the amount of background light detected, thereby increasing the maximum penetration depth.

We present a series of experiments to predict the maximum penetration depth at which typical biological structures in amelanotic tissue can be detected. The behavior of the detected signal is examined as the signal source strength (index of refraction mismatch), the signal source depth, and the medium scattering coefficient are varied. The behavior of the detected background produced by scattering outside the focal volume is examined as the medium scattering coefficient, the depth in the medium, the dimensionless pinhole radius, ν_p, and the shape of the scattering phase function are varied. These results are used to estimate the maximum depth at which biological signal sources can be imaged in unpigmented tissues. Two limits to the maximum penetration depth are considered on the basis of the S/B ratio and the S/N ratio. We show that the background is a strong function of ν_p. When ν_p approaches the ideal confocal performance ($\nu_p \leq 3$), the maximum penetration depth is limited by the S/N ratio to ~3–4 OD's, depending on detector bandwidth, for an index mismatch of 0.05 and a wide range of scattering coefficients. As ν_p increases to 8, the maximum penetration depth is limited by the S/B ratio and is dependent on the scattering coefficient. At $\mu_s = 100\ \text{cm}^{-1}$ (e^{-1} penetration depth, l_s = 100 μm) and $\Delta n = 0.05$, the maximum penetration depth is ~2 OD.

2. Experimental Methods

A confocal reflectometer was constructed as shown in Fig. 1. Illumination light was obtained from a spatially filtered Ti:Sapphire laser at 785 nm. A collimated beam from the spatial filter was focused by a lens (f = 80 mm) 160 mm behind a 25×, 0.8 NA (Zeiss 461625) immersion objective, equipped with an immersion-index correction collar. A 5-mm-diameter beam was chosen to fill the aperture of the objective. The light backscattered from the sample was partially reflected by a beam splitter and focused by a lens (L2) onto a pinhole. In an initial experiment, a 20×, 0.4 NA microscope objective was used to focus the light onto a 5-μm-diameter pinhole to provide a ν_p of 8. Later experiments used a 50.8-mm focal length, 0.05 NA lens to focus the light onto 15-, 25-, and 50-μm-diameter pinholes to provide ν_p of 3, 5, and 10. The light passing through the pinhole was detected by an avalanche photodiode (APD) (Hamamatsu C5460).

Two types of phantoms were investigated with this system: uniform scattering samples and multilayer scattering samples containing a planar refractive-index mismatch. Each experiment consisted of recording the APD voltage as a tissue phantom was scanned along the optical axis through the focus of the confocal system. Measurements of the uniform phantom quantified photons arising from scattering only, referred to as background, whereas those from the second type of phantom quantified contributions from an embedded index mismatch and scattering (signal and background). The difference of these two measurements is a measure of those photons arising from the index mismatch and is referred to as signal. Data were obtained from uniform and multilayer phantoms with different scattering coefficients to characterize the dependence of the signal, the background, and the S/B ratio on the scattering coefficient and the dimensionless pinhole radius ν_p.

The uniform scattering phantom [Fig. 2(a)] consisted of 1-μm-diameter latex microspheres (n = 1.59) suspended in gelatin (n = 1.36). The scattering coefficient of the uniform phantom was varied between 0 and 200 cm^{-1} (l_s = 50 μm) when the concentration of the microspheres was adjusted according to Mie theory.[8] Scattering coefficients were confirmed to be within 10% of the predicted value with spectrophotometer measurement at 785 nm.[9]

The construction of the multilayer phantom, as shown in Fig. 2(b), consists of two uniform scattering layers with equal scattering coefficients but different indices of refraction. The top layer consisted of gelatin (n = 1.36) containing 1-μm-diameter latex spheres. The second layer consisted of immersion

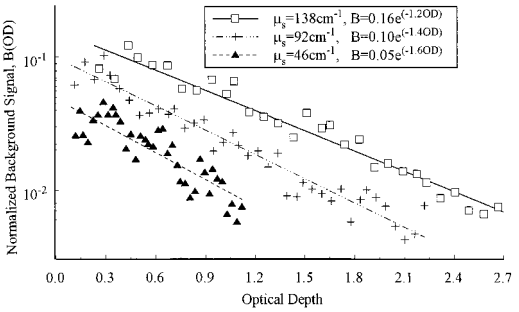

Fig. 3. Processed background signal measured with a ν_p of 8 versus an optical depth for μ_s of 46, 92, and 138 cm^{-1}. The fitted exponential equations (lines) to the data (symbols) appear in the legend.

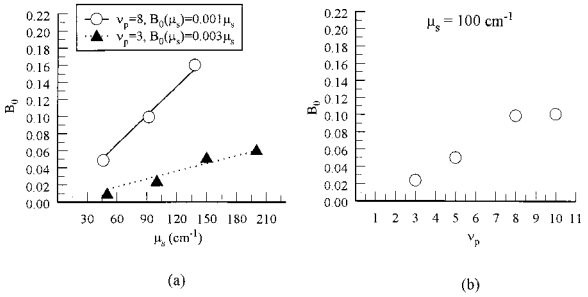

Fig. 4. (a) Dependence of fitted B_0 on the scattering coefficient of the uniform phantom for ν_p of 3 and 8. The fitted linear equations (lines) to the data (symbols) appear in the legend. (b) Dependence of fitted B_0 on ν_p for a scattering coefficient of 100 cm^{-1}.

oil of varying index (1.41 or 1.45) containing a higher density of 1-μm-diameter latex spheres so that both layers had the same scattering coefficient at 785 nm. The resulting index mismatches between the layers of 0.05 and 0.09 are in the range of those reported for cellular components.[10] The thickness and the scattering coefficient of the gelatin layer were varied to adjust the OD at which the planar mismatch was located. An immersion oil (n = 1.41) was used between the microscope objective and the top of the uniform and the multilayer phantoms.

In each experiment, the APD voltage was recorded as a function of focal depth in the sample in steps of 0.3 to 0.6 μm. Data from each phantom were normalized to the signal peak produced by the 0.05 index mismatch at the surface. At least 15 scans were taken, normalized, and averaged together for each multilayer phantom, and at least 25 scans were taken, normalized, and averaged together for each uniform phantom. Data from each average scan were processed in the following manner. The depth scale was corrected for the index mismatch between the immersion fluid and the phantom front surface. The average scan from a similarly processed, uniform, nonscattering phantom (μ_s = 0) was subtracted to remove signal contributions from the 0.05 index mismatch at the surface, contributions from the room lights, and specular reflections from the optics.

3. Experimental Results

Processed scans from uniform phantoms with μ_s from 46 cm^{-1} (l_s = 220 μm) to 138 cm^{-1} (l_s = 73 μm) measured with a ν_p = 8 are shown in Fig. 3 as a function of OD. The background due to scattering decreases exponentially with OD; similar trends were observed at all scattering coefficients, and dimensionless pinhole radii were investigated. In general, the background (B) can be described by Eq. (1), where B_0 is the amplitude of the background at the surface and A_B is the decay coefficient.

$$B(\mathrm{OD}, \mu_s, \nu_p) = B_0(\mu_s, \nu_p)\exp[-A_B(\mu_s, \nu_p)\mathrm{OD}]. \quad (1)$$

All of the processed scans from the uniform phantoms were fit to Eq. (1) with a least-squares fit where B_0 and A_B were free parameters. Data were measured from uniform phantoms with a range of scattering coefficients (50^{-1}–200 cm^{-1}) at a ν_p of 3 and 8. The agreement between the fit (lines) and the data (symbols) in Fig. 3 is typical. Figure 4(a) shows the dependence of B_0 on the scattering coefficient at ν_p = 3 and 8; in general, B_0 increases linearly with increasing scattering coefficient. The lines through the symbols in Fig. 4(a) represent a linear least-squares fit to the data points, which assumes B_0 goes to 0 at μ_s = 0. Figure 4(a) shows that reducing ν_p from 8 to 3 decreases B_0; the reduction is greater at higher scattering coefficients. Data were measured from a uniform phantom with μ_s = 100 cm^{-1} at all dimensionless pinhole radii from 3 to 10. Figure 4(b) shows the dependence of B_0 on ν_p in more detail at μ_s = 100 cm^{-1}. Again, as the dimensionless pinhole radius is reduced, B_0 is reduced. Figure 5(a) shows the dependence of the background decay constant on μ_s at ν_p = 3 and 8; in general, A_B decreases linearly with increasing scattering coefficient. The lines in Fig. 5(a) represent a linear least-squares fit to these data. Note that as the scattering coefficient approaches zero, the decay coefficient is approximately two. As ν_p is reduced from 8 to 3, the decay constant increases. The relationship between A_B and ν_p is depicted in more detail in Fig. 5(b) for μ_s = 100 cm^{-1}.

Figure 6(a) shows a processed scan from a multilayer phantom with μ_s = 138 cm^{-1} and a 0.09 index mismatch located 2.2 OD's beneath the sample sur-

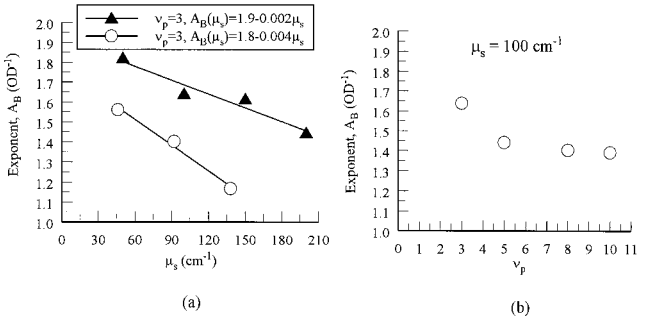

Fig. 5. (a) Dependence of fitted A_B on the scattering coefficient of the uniform phantom for ν_p of 3 and 8. The fitted linear equations (lines) to the data (symbols) appear in the legend. (b) Dependence of fitted A_B on ν_p for a scattering coefficient of 100 cm^{-1}.

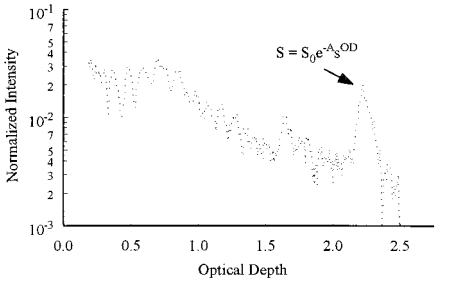

(a)

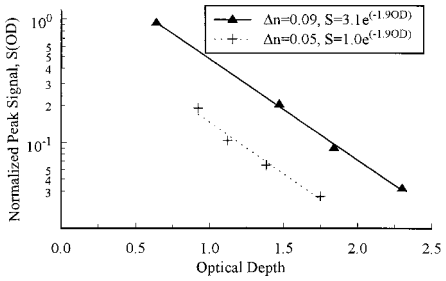

(b)

Fig. 6. (a) Processed scan measured with a ν_p of 8 from a multilayer phantom with a mismatch of 0.09 and a scattering coefficient of 138 cm^{-1}. (b) Processed signal peak amplitude measured with a ν_p of 8 versus optical depth for index mismatches of 0.05 and 0.09. Fitted exponential equations (lines) to the data (symbols) appear in the legend.

face. The scan of the multilayer phantom contains contributions from both the background scattering and the embedded index mismatch. To isolate the index mismatch signal from the background, we subtracted the processed scan from the homogeneous phantom with the same scattering coefficient. With the background contributions removed, the intensity of the detected signal peak from the index mismatch could also be described by a decaying exponential:

$$S(\mathrm{OD}) = S_0 \exp(-A_S \mathrm{OD}), \tag{2}$$

where S_0 is the signal amplitude expected if the index mismatch were located at the sample surface (i.e., no attenuation) and A_S is the decay coefficient. Figure 6(b) shows the measured S as a function of OD (symbols) and the corresponding least-squares fit to Eq. (2) (lines) for index mismatches of 0.05 and 0.09 and a ν_p of 8. In both cases, the signal decreases at approximately exp(−2OD). Because all data were normalized to the 0.05 surface mismatch, S_0 is equal to 1 for the 0.05 mismatch. S_0 is a factor of 3.1 greater for the 0.09 mismatch, which corresponds to the ratio of Fresnel reflection coefficients at normal incidence for the given mismatches. Although changing the dimensionless pinhole radius affects the absolute intensity of the detected signal, all data presented here have been normalized to the 0.05 surface index mismatch, which removes this dependence.

4. Discussion

As demonstrated previously,[5,6] the signal strength decays at approximately exp(−2OD), indicating that the signal photons are produced by single backscattering at the focal volume. The results show an interesting dependence of the background on both the optical properties of the medium and the dimensionless pinhole radius of the system. There are two primary pathways in which a background photon could be produced: (i) single backscattering, which occurs at (or near) the focal volume of the confocal system, or (ii) multiple scattering primarily outside the focal volume, resulting in a photon exiting the tissue with a trajectory appearing to originate in the focal volume. In either case, the background detected at the surface, B_0, would increase linearly with the scattering coefficient of the sample, since the scattering coefficient is proportional to the number of spheres per unit volume. This is consistent with the results in Fig. 4(a).

If the detected background photons are produced through method (i), the background should decay at approximately exp(−2OD) for all pinhole radii, since they would incur the same round-trip attenuation as the signal photons. This is in contrast to what is observed experimentally. Figure 5(a) shows that the background decays at a slower rate than exp(−2OD). The decay constant, A_B, is dependent on the scattering coefficient and the dimensionless pinhole radius. These results suggest that the background photons arise primarily from the second mechanism and that the importance of multiple scattering rises as the scattering coefficient increases and the dimensionless pinhole radius increases. This has important consequences for determining the penetration depth limits for *in vivo* confocal imaging. By reducing the radius of the pinhole, it is possible to decrease the amplitude of the background and increase its decay rate, potentially making greater penetration into the tissue possible.

The maximum penetration is determined by one of two factors: the S/B ratio or the S/N ratio. The data presented in this paper makes it possible to predict the S/B ratio under a variety of conditions. S/B ratio can be calculated from Eqs. (1) and (2) as

$$\frac{S(\mathrm{OD})}{B(\mathrm{OD}, \mu_s, \nu_p)} = \frac{S_0 \exp(-2\mathrm{OD})}{B_0(\mu_s, \nu_p)\exp[-A_B(\mu_s, \nu_p)\mathrm{OD}]} = \frac{S_0}{B_0(\mu_s, \nu_p)} \exp\{-[2 - A_B(\mu_s, \nu_p)]\mathrm{OD}\}, \tag{3}$$

assuming that $A_s = 2$.

If one is limited by the S/B ratio, the maximum penetration depth can then be calculated from Eq. 3 for a given S/B ratio detection limit (S/B_{lim}) as

$$\mathrm{OD}_{\mathrm{Max,S/B}} = \frac{-\ln[(S/B_{lim}B_0)(\mu_s, \nu_p)] + \ln(S_0)}{[2 - A_B(\mu_s, \nu_p)]}. \tag{4}$$

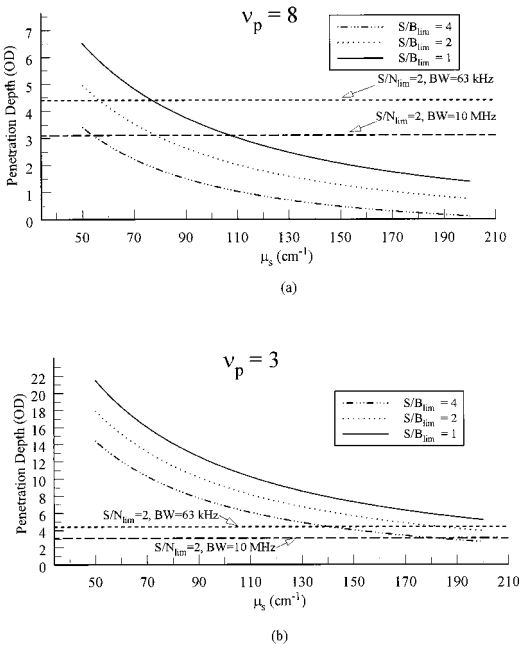

Fig. 7. Maximum penetration depth limits due to S/B ratio limits calculated from Eq. (4) for (a) $\nu_p = 8$, (b) $\nu_p = 3$, and S/B ratio detection limits of 1, 2, and 4. Horizontal lines represent the penetration depth limits due to S/N ratio limits calculated from Eq. (5) for a S/N ratio detection limit of 2 and detector bandwidths of 63 kHz and 10 MHz.

For a 0.05 index mismatch signal source, the amplitude of S_0 is 1 because the data has been normalized to a 0.05 mismatch at the surface. Figure 7 depicts the resulting penetration depth limits to detect a 0.05 mismatch versus the scattering coefficient of the media for a ν_p of 3 and 8 and a range of S/B ratio detection limits. In this calculation, A_B and B_0 were taken from the fitted equations shown in Figs. 4(a) and 5(a).

Limits imposed by the S/N ratio must also be considered. The minimum detectable signal due to electronic noise is given by the product of the detector noise equivalent power (NEP), detector or amplifier gain (G), detector bandwidth (BW), and the S/N ratio detection limit (S/N_{lim}). Assuming the detected signal voltage decays as $V_0 \exp(-2OD)$, the maximum penetration depth can be calculated from Eq. (5).

$$OD_{max,S/N} = \frac{-\ln[(S/N_{lim})NEP(G)(BW)^{1/2}] + \ln(V_0)}{2}. \quad (5)$$

In the experiments reported here, the illumination power of 5 mW provided a signal of approximately 1 V from the 0.05 surface mismatch. For the APD or amplifier combination used (NEP = 0.2 pW/(Hz)$^{1/2}$, G = 1.5 × 10^6 V/W), a sampling BW ($1/\tau_{Sample}$) of 63 kHz, and a $S/N_{lim} = 2$, the minimum detectable signal is 150 μV. As such, a 0.05 mismatch could be detected at a maximum depth of 4.4 OD. Alternatively, with a 10-MHz BW, typical of that used in an imaging system, the maximum penetration depth decreases to 3.1 OD. These limits are shown as horizontal lines in Fig. 7.

Figure 7 shows an interesting consequence of the dependence of the background upon ν_p. In general, the penetration depth is limited by the S/N ratio when μ_s is small or ν_p is small; penetration depth is limited by the S/B ratio when μ_s is large or ν_p is large. At $\nu_p = 8$, for a $\mu_s > 55$ cm^{-1}, Fig. 7(a) predicts that the penetration depth is limited by the S/B ratio. However, when ν_p is reduced to 3 [Fig. 7(b)], the background is sufficiently reduced so that the penetration depth is limited by the S/N ratio for $\mu_s < 180$ cm^{-1}.

The dependence of the signal on ν_p is removed from the results shown here since each scan has been normalized to the signal peak from the 0.05 surface mismatch. However, the detected signal voltage has been shown[11] to decrease theoretically, according to $1 - J_0(\nu_p)^2 - J_1(\nu_p)^2$, where J_n is a Bessel function of the nth kind. When this approximation is used, reducing ν_p from 8 to 3 should reduce the signal by only 12%. However, we have observed experimentally an average reduction of 35–40% in the surface peak voltage by reducing the ν_p from 8 to 3. The discrepancy is most likely due to effects of spherical aberrations.[12] Because the relative signal of the 0.05 and the 0.09 mismatch scaled according to the Fresnel reflection coefficients, it should be possible to estimate the relative signal strengths for other planar index mismatches. For surfaces with a large radius of curvature compared to the lateral resolution, this is a good approximation. For example, the diameter of a typical epithelial cell is approximately 15 μm, which is large compared with the diffraction-limited optical resolution.

In addition to its dependence on ν_p and μ_s, the detected background and thus the S/N ratio will vary depending on the shape of the phase function of the scatterers. To examine this dependence, we compared the detected background measured from a tissue phantom with $\mu_s = 92$ cm^{-1} to the detected background computed from a Monte Carlo simulation in a confocal geometry. The details of the model can be found in Ref. 7. The computed background in which Henyey–Greenstein and Mie theory phase functions are used, is plotted with the measured curve in Fig. 8, where all three are normalized to a value of 1 at the 0.05 surface mismatch. The anisotropy, g, is 0.9 in all cases, although the shape of the phase functions are different.

The measured background matches that computed with the Mie theory phase function more closely than that computed with a Henyey–Greenstein phase function, which overestimates the expected background. Since the scattering in the phantom originates from the embedded polystyrene spheres, the agreement with the Mie phase function is expected. Figure 8 demonstrates that the detected background is sensitive to the shape of the phase function, which is not uniquely described by a single parameter such as the anisotropy.

Other studies[13,14] have indicated that the shape of

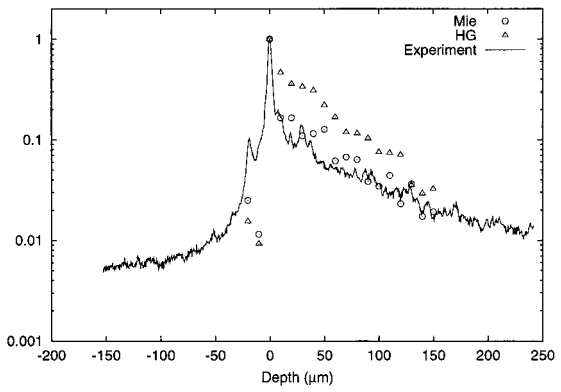

Fig. 8. Comparison of measured background from a tissue phantom (μ_s = 92 cm^{-1}) with the background predicted from a Monte Carlo model with two different phase functions with an anisotropy, g, of 0.9.

the phase function, rather than the anisotropy, is important when measurements are made after only a few scattering events. In tissue, scattering originates from small-scale spatial variations in the index of refraction on the cellular level. The scattering patterns of cells will be different from both Mie theory and Henyey–Greenstein phase functions,[15] and the effects of this phase function on the background must also be considered. Thus computational and measured estimates of the maximum penetration depth of confocal imaging must take into account the shape of the phase functions of tissues to be imaged.

5. Conclusions

Confocal imaging has the potential to image structures deep within highly scattering media, like tissue. Previously, the ability of the confocal technique to penetrate significant depths has been in doubt due to the anticipated levels of background signal from diffusely scattered photons. Our results have shown that the background, although dependent on the scattering coefficient of the medium and the shape of the phase function, can be controlled by the proper choice of pinhole radius. For the range of scattering expected for tissue *in vivo* and when a normalized pinhole radius of $\nu_p = 3$ is used, the background can be sufficiently reduced so that the limit is dependent on the signal-to-noise ratio. As the pinhole radius increases, a confocal system enters a regime where the signal-to-background ratio becomes the limiting factor.

References

1. J. V. Jester, P. M. Andrews, W. M. Petroll, M. A. Lamp, and H. D. Cavanagh, "*In vivo*, real-time confocal imaging," J. Electron Microsc. Tech. **18,** 50–60 (1991).
2. B. Masters and A. A. Thaer, "Real-time scanning slit confocal microscopy of the *in vivo* human cornea," Appl. Opt. **33,** 695–701 (1994).
3. M. Rajadhyaksha, M. Grossman, D. Esterowitz, R. H. Webb, and R. R. Anderson, "*In vivo* confocal scanning laser microscopy of human skin: melanin provides strong contrast," J. Invest. Dermatol. **104,** 946–952 (1995).
4. J. Izatt, M. Hee, and G. Owen, "Optical coherence microscopy in scattering media," Opt. Lett. **19,** 590–592 (1994).
5. J. Schmitt, A. Knuttel, and M. Yadlowsky, "Confocal microscopy in turbid media," J. Opt. Soc. Am. A **11,** 2226–2235 (1994).
6. M. Kempe, W. Rudolph, and E. Welsch, "Comparative study of confocal and heterodyne microscopy for imaging through scattering media," J. Opt. Soc. Am. A **13,** 46–52 (1996).
7. A. K. Dunn, C. Smithpeter, A. Welch, and R. Richards-Kortum, "Sources of contrast in confocal reflectance imaging," Appl. Opt. **35,** 3441–3446 (1996).
8. H. van de Hulst, *Light Scattering by Small Particles* (Dover, New York, 1957).
9. S. Prahl, M. V. Gemert, and A. Welch, "Determining the optical properties of turbid media by using the adding–doubling method," Appl. Opt. **32,** 559–568 (1993).
10. J. Maier, S. Walker, S. Fantini, M. Franceschini, and E. Gratton, "Possible correlation between blood glucose concentration and the reduced scattering coefficient of tissues in the near infrared," Opt. Lett. **19,** 2062–2064 (1994).
11. T. Wilson, "The role of the pinhole in confocal imaging systems," in *Handbook of Biological Confocal Microscopy*, J. Pawley, ed. (Plenum, New York, 1995), pp. 99–113.
12. C. J. Sheppard, M. Gu, K. Brain, and H. Zhou, "Influence of spherical aberration on axial imaging of confocal reflection microscopy," Appl. Opt. **33,** 616–624 (1994).
13. W. Starr, "Light dosimetry *in vivo*," Phys. Med. Biol. **42,** 763–787 (1997).
14. J. Mourant, J. Boyer, A. Hielscher, and I. Bigio, "Influence of the scattering phase function on light transport measurements in turbid media performed with small source–detector separations," Opt. Lett. **21,** 546–548 (1996).
15. A. K. Dunn and R. Richards-Kortum, "Three-dimensional computation of light scattering from cells," IEEE J. Sel. Top. Quantum Electron. **2,** 898–905 (1996).